JOURNAL OF BACTERIOLOGY, Dec. 1999, p. 7531–7544 Vol. 181, No. 24
0021-9193/99/$04.00+0

Genetic and Functional Analyses of the Conserved C-Terminal Core Domain of *Escherichia coli* FtsZ

XIAOLAN MA AND WILLIAM MARGOLIN*

Department of Microbiology and Molecular Genetics, University of Texas—Houston Medical School, Houston, Texas 77030

Received 8 July 1999/Accepted 6 October 1999

In *Escherichia coli*, FtsZ is required for the recruitment of the essential cell division proteins FtsA and ZipA to the septal ring. Several C-terminal deletions of *E. coli* FtsZ, including one of only 12 amino acids that removes the highly conserved C-terminal core domain, failed to complement chromosomal *ftsZ* mutants when expressed on a plasmid. To identify key individual residues within the core domain, six highly conserved residues were replaced with alanines. All but one of these mutants (D373A) failed to complement an *ftsZ* chromosomal mutant. Immunoblot analysis demonstrated that whereas I374A and F377A proteins were unstable in the cell, L372A, D373A, P375A, and L378A proteins were synthesized at normal levels, suggesting that they were specifically defective in some aspect of FtsZ function. In addition, all four of the stable mutant proteins were able to localize and form rings at potential division sites in chromosomal *ftsZ* mutants, implying a defect in a function other than localization and multimerization. Because another proposed function of FtsZ is the recruitment of FtsA and ZipA, we tested whether the C-terminal core domain was important for interactions with these proteins. Using two different in vivo assays, we found that the 12-amino-acid truncation of FtsZ was defective in binding to FtsA. Furthermore, two point mutants in this region (L372A and P375A) showed weakened binding to FtsA. In contrast, ZipA was capable of binding to all four stable point mutants in the FtsZ C-terminal core but not to the 12-amino-acid deletion.

FtsZ plays a key regulatory and structural role during bacterial cell division. It self-assembles into a ring structure on the inner face of the cytoplasmic membrane at the division site and remains at the leading edge of the invaginating septum (6, 28, 33). The FtsZ concentration appears to be an important regulator of its assembly into the ring, because too little FtsZ results in few rings and the formation of nonseptate filaments while a moderate excess of FtsZ results in division at the cell poles in addition to midcell (10, 36). Because the midcell localization of all of the other known essential cell division proteins requires FtsZ, the FtsZ ring is postulated to form the framework that recruits other components of the putative division machinery. FtsZ has been shown to interact directly with FtsA and ZipA (12, 14, 21, 34) and appears to recruit them independently to the FtsZ ring (3, 15, 16, 19). Because many, and perhaps all, of the periplasmic cell division proteins depend upon FtsA for proper localization, and FtsA is well conserved in many bacteria, FtsA may serve as a molecular bridge between the FtsZ ring and the periplasmic proteins.

FtsZ can be thought of as a bacterial cytoskeletal organizer (22). This idea is especially compelling because of the functional and structural homology between FtsZ and tubulin, the key eukaryotic cytoskeletal protein. The crystal structures of FtsZ and tubulin exhibit striking similarities (17). Like tubulin, FtsZ hydrolyzes GTP (11, 25, 31), forms protofilaments in vitro (7, 13) whose assembly depends on GTP (26, 37), and has a similar response to hydrophobic probes (38). The cytoskeletal behavior of FtsZ is also evident in the spiral-shaped septa formed by similarly spiral-shaped FtsZ polymers, indicating that the shape of the FtsZ structure can determine the shape of the resulting septum (2).

* Corresponding author. Mailing address: Department of Microbiology and Molecular Genetics, University of Texas—Houston Medical School, 6431 Fannin, Houston, TX 77030. Phone: (713) 500-5452. Fax: (713) 500-5499. E-mail: margolin@utmmg.med.uth.tmc.edu.

Chloroplasts and nearly all prokaryotes have an FtsZ homolog. Based on sequence alignments among the many species from which it has been isolated, FtsZ can be divided into three major domains: a large, conserved N terminus, a variable linker domain, and a small, highly conserved C terminus. The N-terminal region of approximately 320 residues is highly conserved throughout all FtsZs and includes the GTP binding motif that is also found in tubulins. The crystal structure of *Methanococcus jannaschii* FtsZ shows that residues 38 to 227 in this region form a Rossmann fold-like GTPase domain (17). We previously reported that a truncated *Escherichia coli* FtsZ containing only this N-terminal domain (amino acids 1 to 316) fused to GFP was able to form large fluorescent polymers in vivo and in vitro (19, 37). This indicated that the C terminus is dispensable for polymerization. In contrast, a deletion of 38 residues at the extreme N terminus abolished the localization of FtsZ-GFP protein to rings in vivo, suggesting that the N terminus of FtsZ is essential for ring assembly (19). Similar conclusions have been drawn from yeast two-hybrid studies of self-association of FtsZ (12, 34).

The linker domain is characterized by the variability of its sequence and its length. While this region is fairly short in most organisms, on the order of 40 to 50 amino acids, several α-proteobacterial species contain large linkers of 150 to 200 amino acids that are proline and glutamine rich (23, 29). The specific function of this linker region has not yet been addressed.

Finally, the extreme C-terminal region is variable in length but contains a small consensus sequence of 6 to 8 highly conserved residues that we refer to as the C-terminal core domain (Fig. 1). The core is conserved throughout most bacteria and chloroplasts, but not the archaea. The extreme C terminus of the *M. jannaschii* FtsZ, therefore, lacks the sequence conservation of the bacterial core domains; in addition, it was disordered in the crystal and hence not resolved (17). As a result, the structure and function of the core has not been studied in detail.

SPECIES	FTSZ C-TERMINAL CORE
Escherichia coli	DYLDI**P**AFLR
Pseudomonas aeruginosa	DYLDI**P**AFLR
Agrobacterium tumefaciens	DQLEI**P**AFLR
Bacillus subtilis	DTLDI**P**TFLR
Thermotoga maritima	PEGDI**P**AIYR
Aquifex aeolicus	EEEEI**P**AVIR
Streptococcus pyogenes	DELET**P**PFFK
Mycobacterium tuberculosis	DDVDV**P**PFMR
Streptomyces coelicolor	EELDV**P**DFLK
Enterococcus hirae	ELSTP**P**FFRS
Treponema pallidum	EDLDE**P**TFLR
Corynebacterium glutamicum	DDLDV**P**SFLQ
Mycoplasma pulmonis	QDDTL**P**FFLK
Helicobacter pylori	EELSI**P**TTMR
Physcomitrella patens	SAINI**P**SFLR
Arabidopsis thaliana	GSVEI**P**EFLK

FIG. 1. Alignment of C-terminal core domains of diverse FtsZ homologs; the bottom two are plant chloroplast homologs. The invariant proline residue, corresponding to P375 of *E. coli* FtsZ, is highlighted in boldface. The underlined residues denote residues changed in this study to an alanine. *Arabidopsis thaliana* FtsZ refers to one of at least two chloroplast homologs; the other homolog lacks the homology to the core. Archaeal FtsZs also lack this domain, as do those from other *Mycoplasma* species.

Recently, it was found that a *Caulobacter crescentus* FtsZ with the C-terminal 24 residues, including the core domain, deleted displayed a dominant-negative phenotype and was unable to interact with FtsA in a yeast two-hybrid assay (12). Although this study did not specifically pinpoint the core residues, it suggested that this domain is important for the FtsZ-FtsA interaction. In addition, studies with an FtsZ with the entire C-terminal domain (linker plus core) deleted indicated that either the linker domain, the C-terminal core, or both are required for recruitment of FtsA and/or ZipA (12, 16). However, the core domain was not specifically targeted in these studies.

In this paper, we characterize the functional domains of the C terminus of FtsZ by constructing a series of C-terminal truncations and point mutations in *E. coli ftsZ*. We then test the abilities of these mutant proteins to localize and interact with FtsA and ZipA. Our data suggest that the extreme C terminus of FtsZ is not required for its localization but may be important for its interaction with FtsA and ZipA. Alteration of several consensus residues in the core region appears to affect only the interaction with FtsA. Furthermore, several of these point mutant FtsZs display dominant-negative phenotypes.

MATERIALS AND METHODS

Bacterial strains and growth conditions. *E. coli* strains and plasmids are listed in Table 1. Strain JM105, containing *lacI*^{q} on an F′ plasmid, was used as the wild-type *E. coli* host strain. JFL101 (obtained from J. Lutkenhaus, University of Kansas Medical Center), containing the *ftsZ84*(Ts) allele, was used as the thermosensitive *ftsZ* mutant strain. The *ftsZ* depletion strain, here designated WM746, is WX7/pCX41 (35) and was obtained from W. Cook and L. Rothfield, University of Connecticut Health Center. The standard growth medium was Luria-Bertani (LB) medium, containing 0.5% NaCl, or LBNS, which contains no added NaCl. This medium was supplemented with ampicillin (50 μg per ml), chloramphenicol (20 μg per ml), or tetracycline (10 μg per ml) when needed. *E. coli* wild-type strains were grown at 37°C, while temperature-sensitive strains were grown at 32°C (permissive) or 42 to 44°C (nonpermissive) on LBNS medium containing appropriate antibiotics.

Plasmid construction. The C-terminal truncation mutants of *ftsZ* were generated by PCR amplification. A single forward primer (5′AAGAGCTCGGAGA GAAACTATG) was used, which includes the *ftsZ* native ribosome binding site as well as a *Sac*I site at the 5′ end. The reverse primers were designed to be complementary to the sequences encoding different regions of the FtsZ C terminus and also included a stop codon as well as an *Xba*I site at the 5′ end. Primers for the FtsZ-GFP fusion proteins, corresponding to these C-terminally truncated FtsZ mutants, did not contain a stop codon and were in frame with the sequence encoding the N terminus of GFP. The sequences of the reverse primers for generating these FtsZ C-terminal deletion mutants were as follows: 5′AAT CTAGATTAATAATCCGGCTCTTTCG (ZΔC1), 5′TTTTCTAGATTAGTCA TTCACGACTTTAG (ZΔC1.1), 5′AAATCTAGATTACGGAGCCATCCCAT GC (ZΔC1.2), 5′AAATCTAGATTAAACCTGCTTATTGGTC (ZΔC1.3), and 5′AATCTAGATTAGCCGATACCTGTCGCAAC (ZΔC2). The sequences of the reverse primers for constructing the corresponding FtsZ-GFP fusion proteins were 5′AATCTAGAATAATCCGGCTCTTTCG (ZΔC1), 5′AAATCTAGAG CCGATACCTGTCGCAAC (ZΔC2), 5′AAATCTAGAGATAACCACAGTC GCG (ZΔC3), and 5′AAATCTAGACTCATCCAGACGCAGG (ZΔC4).

E. coli ftsZ derivatives were amplified by PCR from plasmid pZAQ (36) containing *E. coli ftsQAZ*. The PCR products were cleaved with *Sac*I and *Xba*I and cloned into *Sac*I- and *Xba*I-cleaved pBC or pGBC. Derivatives of *ftsZ* were then subcloned into pMK4, a pWM176 derivative that carries a copy of wild-type *ftsZ* between the *Xho*I and *Sac*I sites that is under *tac* promoter control. To replace part of the wild-type *ftsZ* in pMK4, *Kpn*I-*Sma*I fragments of *ftsZ* derivatives in pBC were ligated to *Kpn*I/*Ecl*136II-cleaved pMK4.

Point mutations in *ftsZ* were generated by site-directed mutagenic PCR as previously described (8). The sequences of the mutagenic primers were 5′CGA AAGAGCCGGATTATGCGGATATCCCAGCATTCC for ZL372A, 5′GATT ATCTGGATATCGCAGCATTCCTGCG for ZD373A, 5′CGGATTATCTGG ATGCCCCAGCATTCCTGCGTAAG for ZI374A, 5′GCCGGATTATCTGGC TATCCCAGCATTCC for ZP375A, 5′TATCTGGATATCCCAGCAGCCCTG CGTAAGCAAGCTG for ZF377A, and 5′GGATATCCCAGCATTCGCGCG TAAGCAAGCTGATTAA for ZL378A. The PCR products were digested with *Bst*EII and *Cla*I to yield fragments of approximately 600 bp, of which 200 bp encode the C terminus of FtsZ. These fragments were then cloned into the *Bst*EII and *Cla*I sites of pZG, a derivative of pBC that carries *ftsZ*-GFP, to replace the sequence encoding the corresponding region of *ftsZ* and the downstream GFP coding region with the point mutations. All the point mutations were confirmed by DNA sequencing. To move the mutant *ftsZ*s residing in pZG to pMK4, the plasmids were digested first with *Xho*I, followed by a fill in of the *Xho*I overhang with Klenow fragment, and then digested with *Kpn*I. The fragments harboring the mutant *ftsZ*s were subcloned into *Kpn*I/*Ecl*136II-cleaved pMK4. The expression and integrity of FtsZ mutants were confirmed by immunoblotting with affinity-purified polyclonal anti-FtsZ.

The *zipA* gene was amplified by PCR directly from *E. coli* genomic DNA with the upstream primer 5′AAGAGCTCAACAGAGAATATAATGATG and the downstream primer 5′AATCTAGAGGCGTTGGCGTCTTTG. The PCR fragment was cleaved with *Sac*I and *Xba*I and cloned into the *Sac*I and *Xba*I sites of a derivative of pGBC that contains a copy of *lacI*^{q} at the *Eco*RI site. This procedure placed *zipA* under *lac* control and in frame with the downstream GFP coding sequence. To place *zipA*-GFP under arabinose regulation, it was subcloned into pBAD30 between the *Sac*I and *Sal*I sites.

Complementation tests. To test the function of the FtsZ mutant alleles, we transformed the versions cloned in pWM176 into JFL101 and WM1099, an *ftsZ84*(Ts) mutant and an *ftsZ* depletion strain, respectively. Because pWM176 derivatives and the original *ftsZ* depletion strain, WM746, were both tetracycline resistant (Tet^r), WM746 was made Tet^s by replacing the linked Tet^r marker in *leu* with a Kan^r marker from CAG12131 by P1 transduction; the resulting strain became WM1099.

For complementation experiments, derivatives of pWM176 in JFL101 were tested for colony growth on LBNS agar containing 10 to 40 μM isopropyl β-D-thiogalactoside (IPTG) at both 32 and 42°C. For pWM176 derivatives in WM1099, colony growth was tested on LB agar with tetracycline and 5 to 20 μM IPTG at both 32 and 44°C. IPTG concentrations above 20 μM caused significant inhibition of colony growth at both 32 and 44°C in WM1099 derivatives carrying plasmids expressing *ftsZ*. Because *ftsZ* depletion takes several cell cycles to occur, background growth was often observed for the WM1099 and WM1099/pWM176 controls at 44°C.

Immunoblot analysis. JFL101 cells containing the *ftsZ* derivatives in pWM176 were grown at 30°C to exponential phase and then induced with 10 μM IPTG for 90 min at 42°C. JM105 cells harboring the same plasmids were induced with 5 μM IPTG for 3 h at 37°C. The cells were then collected, and total protein was quantitated with the bicinchoninic acid protein assay (Pierce). A total of 25 μg of protein for each sample was separated on sodium dodecyl sulfate–12% polyacrylamide gels and transferred to nitrocellulose membranes (0.45-μm pore size; Micron Separations Inc.). The amplified alkaline phosphatase Immuno-Blot Kit (Bio-Rad) was then used for immunoblotting. Purified anti-FtsZ antiserum at 1:200 dilution was used as the primary antibody, and biotinylated goat anti-rabbit immunoglobulin G at 1:1,000 dilution was used as the secondary antibody.

Yeast two-hybrid analysis. The *Saccharomyces cerevisiae* host strain L40 carries a LexA binding DNA sequence fused with *lacZ* on the chromosome, so the expression of *lacZ* can be activated upon binding of LexA (5). The plasmids used were pACT2.2, containing the GAL4 activation domain (obtained from S. Elledge, Baylor College of Medicine), and pLEXA, containing the LexA DNA binding domain (obtained from J. Jones, M. D. Anderson Cancer Center). To clone *ftsA* into pLEXA, *ftsA* was amplified by PCR, using 5′AAACATATGAT CAAGGCGACGGAC as the upstream primer and 5′TTTGGATCCTTAAAA CTCTTTTCGC as the downstream primer. The PCR product was digested with

TABLE 1. Strains and plasmids used in this study

Bacterial strain or plasmid	Relevant characteristics	Source and/or reference
JM105	F′ *traD36 lacI*^{q} Δ(*lacZ*)M15 *proA*$^+$*B*$^+$/*thi rpsL endA sbcB15 hsdR4* Δ(*lac proAB*)	Laboratory collection
JFL101	*ftsZ84 recA lacY*	18
WM746	WX7 (*ftsZ* frameshift mutant) containing pCX41 (temperature-sensitive plasmid carrying *ftsZ*)	35
CAG12131	*leu*::Tn*5*	Laboratory collection
WM1099	Tet^s version of WM746; WM746 × P1 (CAG12131; *leu*::Tn*5*)	Laboratory collection
WM1221	WM1099 containing pWM1206 + pWM176; Tet^r Amp^r	This work
WM1222	WM1099 containing pWM1206 + pMK4; Tet^r Amp^r	This work
WM1223	WM1099 containing pWM1206 + pWM737; Tet^r Amp^r	This work
WM1224	WM1099 containing pWM1206 + pWM930; Tet^r Amp^r	This work
WM1225	WM1099 containing pWM1206 + pWM931; Tet^r Amp^r	This work
WM1226	WM1099 containing pWM1206 + pWM932; Tet^r Amp^r	This work
WM1227	WM1099 containing pWM1206 + pWM1201; Tet^r Amp^r	This work
WM1228	WM1099 containing pWM1206 + pWM1202; Tet^r Amp^r	This work
WM1229	WM1099 containing pWM1206 + pWM738; Tet^r Amp^r	This work
WM1230	WM1099 containing pWM1206 + pWM1203; Tet^r Amp^r	This work
WM1231	WM1099 containing pWM1206 + pWM739; Tet^r Amp^r	This work
WM1232	WM1099 containing pWM1206 + pWM1204; Tet^r Amp^r	This work
WM1233	WM1099 containing pWM1206 + pWM1205; Tet^r Amp^r	This work
WM1234	JFL101 containing pWM633 + pWM176; Cam^r Tet^r	This work
WM1235	JFL101 containing pWM633 + pMK4; Cam^r Tet^r	This work
WM1236	JFL101 containing pWM633 + pWM737; Cam^r Tet^r	This work
WM1237	JFL101 containing pWM633 + pWM930; Cam^r Tet^r	This work
WM1238	JFL101 containing pWM633 + pWM931; Cam^r Tet^r	This work
WM1239	JFL101 containing pWM633 + pWM932; Cam^r Tet^r	This work
WM1240	JFL101 containing pWM633 + pWM1201; Cam^r Tet^r	This work
WM1241	JFL101 containing pWM633 + pWM1202; Cam^r Tet^r	This work
WM1242	JFL101 containing pWM633 + pWM738; Cam^r Tet^r	This work
WM1243	JFL101 containing pWM633 + pWM1203; Cam^r Tet^r	This work
WM1244	JFL101 containing pWM633 + pWM739; Cam^r Tet^r	This work
WM1245	JFL101 containing pWM633 + pWM1204; Cam^r Tet^r	This work
WM1246	JFL101 containing pWM633 + pWM1205; Cam^r Tet^r	This work
Plasmid		
pBAD30	*araBAD* promoter vector; p15A origin; Amp^r	Laboratory collection
pBCIISK	*colE1* cloning vector; Cam^r	Stratagene
pBC (SK$^+$)	*colE1* cloning vector; Cam^r	Stratagene
pZAQ	pBR322 containing *ftsQAZ* insert between *Pst*I and *Cla*I; Tet^r	36
pZG	Cam^r; *ftsZ*-GFP cloned between *Sac*I and *Pst*I sites in pBC SK(+)	19
pGBC	Cam^r; GFP cloned between *Bam*HI and *Xba*I sites in pBC SK(+)	21
pWM707	Cam^r; *ZΔC1* inserted between *Sac*I and *Xba*I sites in pGBC	This work
pWM630	Cam^r; pGBC-*ZΔC2*	19
pWM766	Cam^r; pGBC-*ZΔC3*	This work
pWM767	Cam^r; pGBC-*ZΔC4*	This work
pWM1206	Amp^r; *zipA*-GFP-*lacI*^{q} fragment cloned between *Sac*I and *Sal*I sites of pBAD30	This work
pWM1207	Amp^r; pBluescript containing *ftsA* and *lacI*^{q}	This work
pWM633	Cam^r; pGBC containing *ftsA*-GFP and *lacI*^{q}	This work
pWM176	Tet^r; IncP cloning vector containing the *tac* promoter	24
pMK4	Tet^r; *E. coli* wild-type *ftsZ* inserted at *Xho*I and *Sac*I sites of pWM176	24
pWM737	Tet^r; pWM176-*ZΔC1*	This work
pWM930	Tet^r; pWM176-*ZΔC1.1*	This work
pWM931	Tet^r; pWM176-*ZΔC1.2*	This work
pWM932	Tet^r; pWM176-*ZΔC1.3*	This work
pWM1201	Tet^r; pWM176-*ZΔC2*	This work
pWM1202	Tet^r; pWM176-*ZL372A*	This work
pWM738	Tet^r; pWM176-*ZD373A*	This work
pWM1203	Tet^r; pWM176-*ZI374A*	This work
pWM739	Tet^r; pWM176-*ZP375A*	This work
pWM1204	Tet^r; pWM176-*ZF377A*	This work
pWM1205	Tet^r; pWM176-*ZL378A*	This work
pWM1208	pLEXA-*ftsA*	This work
pXZE209a	pACT2.2-*virE* (from *A. tumefaciens*)	P. Christie
pWM1209	pACT2.2-*ftsZ*	This work
pWM1210	pACT2.2-*ZΔC1*	This work
pWM1211	pACT2.2-*ZΔC1.1*	This work
pWM1212	pACT2.2-*ZΔC1.2*	This work
pWM1213	pACT2.2-*ZΔC1.3*	This work
pWM1214	pACT2.2-*ZΔC2*	This work
pWM1215	pACT2.2-*ZL372A*	This work
pWM1216	pACT2.2-*ZD373A*	This work
pWM1217	pACT2.2-*ZI374A*	This work
pWM1218	pACT2.2-*ZP375A*	This work
pWM1219	pACT2.2-*ZF377A*	This work
pWM1220	pACT2.2-*ZL378A*	This work

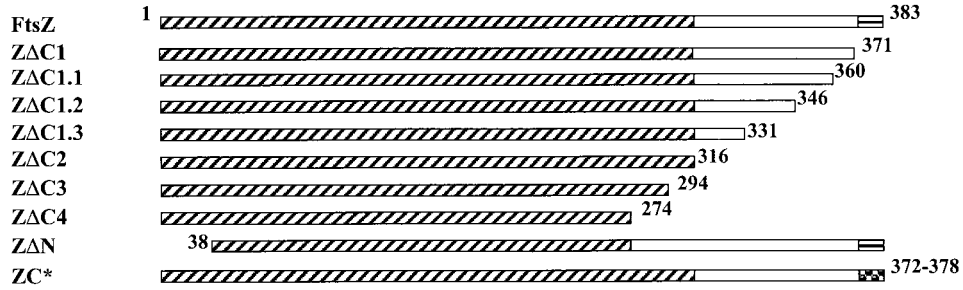

FIG. 2. FtsZ truncation and point mutant derivatives. ZC* represents six mutants with single-residue changes in the C-terminal core. Slanted hatches represent the N-terminal conserved domain, horizontal hatches represent the C-terminal core, and the checkered pattern indicates the C-terminal core that contains mutations. The numbers indicate the beginning or ending residues relative to those of wild-type FtsZ. ZΔC2, ZΔC3, ZΔC4, and ZΔN all contain C-terminal GFP fusions (see Materials and Methods).

*Nde*I, followed by fill in of the overhangs with Klenow fragment and digestion with *Bam*HI. The cleaved product was ligated to *Sma*I/*Bam*HI-cleaved pLEXA, and the resulting plasmid was designated pWM1208. For cloning *ftsZ* into pACT2.2, *ftsZ* was amplified by PCR with 5′AACATATGTTGAACCAATGG AAC as the upstream primer and 5′AAGGATCCATCAGCTTGCTTACGC as the downstream primer. The PCR fragment was cleaved with *Nde*I and *Bam*HI and cloned into the *Nde*I and *Bam*HI sites of pBCIISK(+). The C-terminal *ftsZ* mutant alleles were cloned into the same vector by replacing the C-terminal coding region of *ftsZ* in pBCII-*ftsZ* between the *Sac*II site within *ftsZ* and the *Bam*HI site. The *ftsZ* gene and its mutant derivatives were subcloned between the *Nde*I and *Bam*HI sites on pACT2.2. These two plasmids (pWM1208 and pACT2.2-*ftsZ* or its derivatives) were then transformed into the yeast reporter strain L40. β-Galactosidase activities were estimated by using a filter assay, with X-Gal (5-bromo-4-chloro-3-indolyl-β-D-galactopyranoside) as a substrate (4).

Microscopic techniques. Immunofluorescence staining in combination with phase-contrast imaging and nucleoid staining with 4′,6-diamidino-2-phenylindole (DAPI) were carried out as described previously (39) with minor modifications. The concentration of lysozyme used to permeabilize the cells was varied from 0.8 to 2 mg per ml for different strains to obtain the best results. For FtsZ staining, we used affinity-purified anti-FtsZ at a final dilution of 1:20. To stain FtsA-GFP or ZipA-GFP, polyclonal anti-GFP antiserum was used at a 1:200 dilution. To generate the anti-GFP, we purified GFP from a strain carrying the mut2GFP-overproducing plasmid (9). The antigen was sent to Cocalico Biologicals Inc. (Reamstown, Pa.) for antibody production in rabbits. Anti-FtsZ was similarly obtained from rabbits by using purified overproduced *E. coli* FtsZ as an antigen and was subsequently affinity purified. All microscopic images were taken on an Olympus BX60 microscope, captured in RGB mode with an Optronics DEI-750 camera and a Scion CG-7 frame grabber, and manipulated in Adobe Photoshop. The images were changed to grayscale mode for publication.

RESULTS

Function of C-terminal deletions of FtsZ. To identify the C-terminal domains of *E. coli* FtsZ required for in vivo function, we constructed a series of C-terminal deletions of *E. coli ftsZ* (Fig. 2) and placed them under the control of the IPTG-inducible *tac* promoter in the IncP plasmid derivative pWM176 (24). We first examined whether the mutant *ftsZs* were capable of complementing the *ftsZ84* temperature-sensitive strain JFL101, which is nonviable at 42°C. A strain containing pMK4 (pWM176 carrying the wild-type *ftsZ*) was unable to form colonies on LBNS plates at 42°C in the absence of IPTG, indicating that uninduced expression of *ftsZ* from the plasmid was insufficient to support cell division. Therefore, different IPTG concentrations were used to induce complementing levels of FtsZ. In a range of 10 to 40 μM IPTG, strains harboring pMK4 but not pWM176 formed fast-growing colonies with normal plating efficiency at 42°C, confirming complementation of the *ftsZ84* mutant by the wild-type *ftsZ* on pMK4. When identical induction conditions were used with the deletion derivatives, none of these, including an N-terminal-deletion control, were able to complement *ftsZ84* (Table 2).

To verify these results, we performed similar complementation tests in an *ftsZ* depletion strain, WM1099. The chromosomal copy of *ftsZ* in this strain is inactivated by a frameshift mutation, and viability depends upon an additional copy of *ftsZ* on a plasmid that is temperature sensitive for replication (35). The *ftsZ* plasmid pMK4 or its deletion derivatives were introduced into WM1099, and growth of the transformants was examined at both 32 and 44°C. In the presence of 5 μM IPTG, growth of WM1099 containing pMK4 (wild-type *ftsZ*) was no longer temperature sensitive, whereas WM1099 containing the vector control (pWM176) or any of the *ftsZ* deletion mutants failed to form colonies with normal efficiency at 44°C. In summary, all the deletion mutants were defective in complementing either the *ftsZ* null or the *ftsZ84*(Ts) mutant (Table 2).

Interestingly, one of the *ftsZ* deletion mutants, ZΔC1.1 (remaining amino acids, 1 to 360), exhibited a dominant-negative phenotype when expressed in the wild-type strain JM105 or in JFL101 (*ftsZ84*). Colonies carrying pWM930 (ZΔC1.1) grew very poorly on LB plates at 32°C with 20 μM or higher concentrations of IPTG. When inoculated into LB broth with 5 μM IPTG, cells carrying pWM930 started filamenting and reached an average length of 8 cell units after 3 h of growth. In contrast, under the same induction conditions, cells expressing wild-type *ftsZ* from pMK4 or other truncation mutants remained normal in length (data not shown).

Function of point mutations in the C-terminal core of FtsZ. The failure of ZΔC1 (amino acids 1 to 371; pWM737), which lacks only the C-terminal 12 residues, to complement the *ftsZ84*(Ts) or the *ftsZ* null mutant suggested that residues 372 to 383 are essential for the full function of FtsZ. Sequence alignments of FtsZs from different species revealed that this extreme C terminus is quite highly conserved, with at least 6 residues present in most FtsZs and a central proline residue,

TABLE 2. Summary of complementation and dominant-negative effects of FtsZ derivatives

Derivative[a]	Complementation	Dominant-negative effects
FtsZ	+	−
ZΔC1	−	−
ZΔC1.1	−	+
ZΔC1.2	−	−
ZΔC1.3	−	−
ZΔC2	−	−
ZL372A	−	+
ZD373A	+	−
ZI374A*	−	+
ZP375A	−	+
ZF377A*	−	−
ZL378A	−	−

[a] * indicates that the FtsZ derivative is unstable.

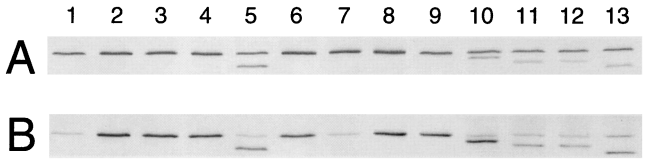

FIG. 3. Western blot analysis of FtsZ and its derivatives expressed in JM105 (wild type) and JFL101 (*ftsZ84*). (A) JM105 derivatives were grown exponentially at 37°C and then induced with 5 μM IPTG for 180 min. (B) JFL101 derivatives were grown at 42°C for 30 min before being induced with 10 μM IPTG for 90 min. The cells were then collected, and total protein was quantitated by bicinchoninic protein assay (Pierce). An equivalent amount of protein (25 μg) was loaded onto each lane, followed by sodium dodecyl sulfate-polyacrylamide gel electrophoresis and immunoblotting. Lane 1, cells containing pWM176; lane 2, pMK4 (wild-type *ftsZ*); lane 3, pWM1202 (*ZL372A*); lane 4, pWM738 (*ZD373A*); lane 5, pWM1203 (*ZI374A*); lane 6, pWM739 (*ZP375A*); lane 7, pWM1204 (*ZF377A*); lane 8, pWM1205 (*ZL378A*); lane 9, pWM737 (*ZΔC1*); lane 10, pWM930 (*ZΔC1.1*); lane 11, pWM931 (*ZΔC1.2*); lane 12, pWM932 (*ZΔC1.3*); lane 13, pWM1201 (*ZΔC2*).

corresponding to P375 of *E. coli* FtsZ, that is particularly well conserved (Fig. 1). To identify the critical amino acids in this region, we constructed six *ftsZ* mutant alleles with each conserved residue individually changed to alanine (Fig. 2). Five of these point mutants (ZL372A, ZI374A, ZP375A, ZF377A, and ZL378A) failed to complement either the *ftsZ84*(Ts) or the *ftsZ* null mutant (Table 2). Three mutant FtsZ derivatives (ZL372A, ZI374A, and ZP375A) exhibited a dominant-negative phenotype similar to that of ZΔC1.1 (Table 2).

In addition, ZI374A and ZF377A were unstable. By immunoblotting with anti-FtsZ antibodies, we found that cells synthesizing ZI374A displayed a truncated polypeptide that was approximately 4 to 5 kDa smaller than wild-type FtsZ protein (Fig. 3, lane 5). ZF377A was largely degraded in both JFL101 (*ftsZ84*) and the WM1099 depletion strain at 42°C (Fig. 3B, lane 7, and data not shown), with a 10-kDa band visible on immunoblots (data not shown). Interestingly, however, ZF377A was synthesized as a full-length protein in the wild-type JM105 strain at either 32 or 42°C (Fig. 3A, lane 7, and data not shown). As mentioned above, ZI374A, although truncated, was very toxic to both wild-type JM105 and JFL101 (*ftsZ84*) cells and therefore was judged to have a dominant-negative effect similar to that of ZΔC1.1.

To ensure that differences in complementation and dominant-negative effects were not caused by significant variations in protein levels, we measured cellular protein levels in JM105 and JFL101 containing the various *ftsZ* plasmids. After induction with 5 μM IPTG for 3 h, cells of the JM105 wild-type strain expressing the wild-type FtsZ (from pMK4) were 1 to 2 cell units in length, whereas cells synthesizing dominant-negative mutant proteins (ZL372A, ZI374A, ZP375A, and ZΔC1.1) had already formed filaments with an average cell length of 8 cell units. Cells expressing other mutant *ftsZ*s, defined as not being dominant negative, were roughly 2 cell units in length. After this microscopic inspection, the FtsZ levels from these cells were measured by immunoblotting. The results indicated that the cellular levels of different FtsZ derivatives in JM105, as normalized to total cell protein, did not vary significantly (Fig. 3A). The levels of the deletion derivatives (Fig. 3A, lanes 10 to 13 [lower bands]) appeared to be consistently lower than those of the point mutants (lanes 4, 6, 7, 8 [which include both endogenous FtsZ and the point mutant FtsZs in the same band] and lane 5 [lower band]) as judged by band intensities. We suspect that one reason for lower signals from the deletions might be that the majority of antigenic epitopes on FtsZ are at the C terminus; deletion of this region might result in less efficient cross-reactivity with the polyclonal antibodies. The FtsZ band intensities on the immunoblots were quantitated and found to be approximately 40 to 70% of the level of the endogenous FtsZ. These results suggest that ZL372A, ZI374A, ZP375A, and ZΔC1.1 negatively affect cell division not because they are present at abnormally high levels but because they interfere with the function of the wild-type protein when they are at similar levels. In contrast, wild-type FtsZ only inhibits division when overproduced to higher than sevenfold native levels (36).

In the case of JFL101 derivatives, immunoblots consistently revealed an approximately threefold-lower level of endogenous FtsZ84 compared to that of endogenous FtsZ in JM105 cells at 42°C (compare lanes 1 in Fig. 3A and B) as well as 32°C (data not shown). As a result, levels of the mutant FtsZ proteins expressed in JFL101 appeared to be approximately sixfold higher than the endogenous FtsZ84, even though most were at about the same absolute levels as in JM105 (compare lanes 2 to 6, 8 to 9, and 11 to 13 in Fig. 3A and B). Only ZΔC1.1 seemed to be at higher levels in JFL101 than in JM105 (compare lanes 10 in Fig. 3A and B), and, as mentioned earlier, ZF377A was degraded only in JFL101 (compare lanes 7 in Fig. 3A and B). The significance of the lower FtsZ84 levels is unclear, although this could be a factor in its thermosensitivity. Nevertheless, our data still indicate that the failure of some of our FtsZ mutant proteins to complement is not because their levels in the cell were inappropriately high or low.

Localization patterns of FtsZ mutant derivatives. When synthesized from plasmids, GFP-tagged FtsZ derivatives lacking the N-terminal 38 residues (ZΔN, containing amino acids 38 to 383) (19), the C-terminal 89 residues (ZΔC3 with amino acids 1 to 294), or the C-terminal 119 residues (ZΔC4 with amino acids 1 to 274) did not exhibit detectable fluorescent foci or rings in cells and instead displayed unlocalized fluorescence (data not shown). These observations, summarized in Table 3, suggest that residues 1 to 316 may be required for the proper localization of FtsZ to division sites.

To investigate the role of the C-terminal 67 residues (amino acids 317 to 383) in the proper targeting of FtsZ to the division site, we determined the subcellular localization of our short FtsZ C-terminal deletions (ZΔC1 and ZΔC2) and point mutants. To distinguish between the cloned mutant FtsZs and the endogenous native FtsZ, we monitored the localization patterns of FtsZs synthesized from pWM176 derivatives in the *ftsZ84*(Ts) strain JFL101 and the *ftsZ* depletion strain WM1099. For JFL101, it was essential to completely inactivate the endogenous FtsZ (FtsZ84), which is defective in GTPase

TABLE 3. Localization of FtsZ derivatives to division sites

Derivative	Localization between separated nucleoids[a]
FtsZ	+
ZΔC1	+
ZΔC1.1	+
ZΔC1.2	+
ZΔC1.3	+
ZΔC2	+
ZΔC3	−
ZΔC4	−
ZΔN	−
ZL372A	+
ZD373A	+
ZI374A	+
ZP375A	+
ZL378A	+

[a] +, present; −, absent.

activity but can form functional FtsZ rings on its own at temperatures below 42°C (1, 11, 31). FtsZ84 rings disappear within 2 min after cells are incubated at 42°C (1). Therefore, to ensure the endogenous FtsZ84 was inactivated, we grew cells at 42°C for 30 min before inducing expression of the cloned mutant *ftsZ* derivatives with 10 μM IPTG for 60 min. The localizations of cloned FtsZ derivatives were examined by immunofluorescence microscopy (IFM) with anti-FtsZ antibodies. Under the conditions used, both wild-type and mutant FtsZs (except the unstable ZF377A) could localize to potential division sites, which were revealed by simultaneously staining nucleoids with DAPI (Fig. 4). All the mutant proteins (except ZF377A) were able to form rings, as judged from the sharp fluorescent bands observed between nucleoids. Fig. 4C, showing ZL372A, and D, showing ZΔC1.3, represent typical patterns for point and deletion mutants, respectively, and were similar to those exhibited by wild-type FtsZ expressed from pMK4 (Fig. 4B) except that cells with pMK4 could divide. In contrast, cells containing the pWM176 vector control exhibited unlocalized fluorescence only (Fig. 4A). The formation of FtsZ rings by the truncated ZI374A under the same conditions (data not shown) suggests that residues 1 to 316 are still present in this truncated version.

For FtsZ to be significantly depleted in strain WM1099, it was necessary to rapidly deplete the temperature-sensitive plasmid (pCX41) that carries a copy of the *ftsZ* gene. WM1099 cells were grown at 42°C for 5 h until they became extremely filamentous (approximately 32 cell units long on average) or when the endogenous FtsZ protein was no longer detectable as bands on immunoblots (data not shown) or by IFM (Fig. 5A). At this time point, expression of the *ftsZ* mutant alleles carried on pWM176 was induced with 5 μM IPTG for 40 min. Cells expressing most of the mutant FtsZ proteins and the pWM176 vector control remained filamentous, as expected (Fig. 5A″, C″, D″). In contrast, expression of wild-type FtsZ from pMK4 induced rapid cell divisions and usually led to cells with normal length (Fig. 5B″), indicating that cell division could be restored in these depleted cells. ZD373A, although it complemented both *ftsZ84* and the *ftsZ* null mutant for colony formation on plates, only induced divisions of some cells while many cells remained filamentous (data not shown). This result is consistent with the idea that colony formation is a less stringent measurement of normal cell division function than direct observation of individual dividing cells.

We also used IFM to investigate FtsZ localization in the *ftsZ* depletion strain WM1099. Cells synthesizing the FtsZ point mutant derivatives (with the exception of the unstable ZI374A and ZF377A proteins) exhibited regularly spaced sharp bands (Fig. 5C, showing immunostaining of ZL372A). These bands were presumably FtsZ rings and appeared similar to bands in cells synthesizing wild-type FtsZ from pMK4 (Fig. 5B). Cells containing the pWM176 vector exhibited only weak unlocalized fluorescence (Fig. 5A). The FtsZ bands were located at potential division sites between nucleoids, as shown by double staining for FtsZ and nucleoids with DAPI. The FtsZ deletion derivatives (ZΔC1, ΔC1.1 to -1.3, and ΔC2, all containing residues 1 to 316) and ZI374A were also able to localize regularly to potential division sites; the frequency of localization, defined as the number of rings per unit cell length, was proportional to the level of induction by IPTG (data not shown). Interestingly, however, these FtsZ derivatives appeared as dots (Fig. 5D, showing ZΔC1.3) rather than the sharp bands formed by the same derivatives synthesized in JFL101 (Fig. 4D). Therefore, it appears that FtsZ deletion mutants containing at least residues 1 to 316 are able to localize to division sites in either strain background but at 42°C they can form clear rings only in JFL101. A summary of the localization results is shown in Table 3.

Protein-protein interactions between FtsA and FtsZ deletion derivatives. To examine interactions between FtsA and FtsZ mutant derivatives, we developed a simple and novel in vivo protein-protein interaction assay. This assay was based on our previous observations that when FtsA-GFP is co-overproduced with FtsZ, fluorescent spiral structures assemble throughout the cell. Similar spirals are often found after overproduction of FtsZ-GFP, but not after overproduction of FtsA-GFP. Because FtsZ-GFP, but not FtsA-GFP, was able to form extensive spirals when overexpressed, we previously postulated that fluorescent spirals in cells overproducing FtsA-GFP and FtsZ resulted from association of FtsA-GFP with FtsZ polymers (24). This assay was then used to test interspecies FtsZ-FtsA interactions in situ and revealed a significantly stronger interaction between rhizobial FtsA-GFP and its cognate FtsZ than with *E. coli* FtsZ (21).

For the present study, we used this assay to determine whether FtsA-GFP could bind to spiral polymers assembled by our mutant FtsZ derivatives. In this system, the *ftsA*-GFP fusion was under the control of the IPTG-inducible *lac* promoter in pBC, a *colE1* plasmid derivative. As with the complementation and localization experiments described above, expression of wild-type *ftsZ* or its mutant alleles was driven by the *tac* promoter in the compatible IncP plasmid, pWM176. JFL101 (*ftsZ84*) cells harboring both *ftsA*-GFP and *ftsZ* were grown at 32°C until they reached early exponential phase and then shifted to 42°C for 30 min to inactivate the endogenous FtsZ84. Overproduction of FtsA-GFP and FtsZ or its derivatives was subsequently induced with 200 μM IPTG for 1 h at 42°C. The cellular structures formed by these proteins were examined by IFM, using anti-GFP and anti-FtsZ to detect FtsA-GFP and FtsZ derivatives, respectively.

In control cells expressing FtsA-GFP and wild-type FtsZ, immunostaining of FtsA-GFP revealed spiral structures that were identical to those previously visible in live cells by GFP fluorescence (19) (Fig. 6B). In contrast, when synthesized in combination with any of the truncated FtsZ derivatives, FtsA-GFP immunostaining revealed only diffuse fluorescence (Fig. 6E, showing ZΔC1). Weak spiral-like patterns that were not easily discernible above background fluorescence were often observed in these cells. These patterns could have been caused by nonspecific staining with anti-GFP, because a high fluorescence background was usually seen even in cells expressing only GFP or FtsA-GFP in the absence of functional FtsZ (Fig. 6A and data not shown). It is also possible that FtsZ84 might be able to copolymerize with the mutant FtsZ proteins, resulting in some FtsA-GFP binding. Staining of parallel samples of cells expressing the truncation mutant with anti-FtsZ revealed mostly fluorescent spirals (Fig. 6E′, showing ZΔC1), although the delineation of the structures was not as sharp as with FtsA-GFP in FtsZ-producing cells visualized with anti-GFP (Fig. 6B). The simplest explanation for these observations is that the C-terminal truncation mutants of FtsZ were able to form spiral polymers but unable to recruit FtsA-GFP efficiently to the polymers. This in turn suggests that the 12-amino-acid C-terminal core domain of FtsZ is important for efficient interaction with FtsA-GFP.

Protein-protein interactions between FtsA and FtsZ point mutant derivatives. This possibility prompted us to test the interactions between FtsA-GFP and the C-terminal core point mutants of FtsZ in the same assay. When stained with anti-FtsZ, cells overproducing wild-type FtsZ (Fig. 6B′) or any of the FtsZ point mutants (Fig. 6C′ and D′ and data not shown), except the unstable mutants ZI374A and ZF377A, exhibited

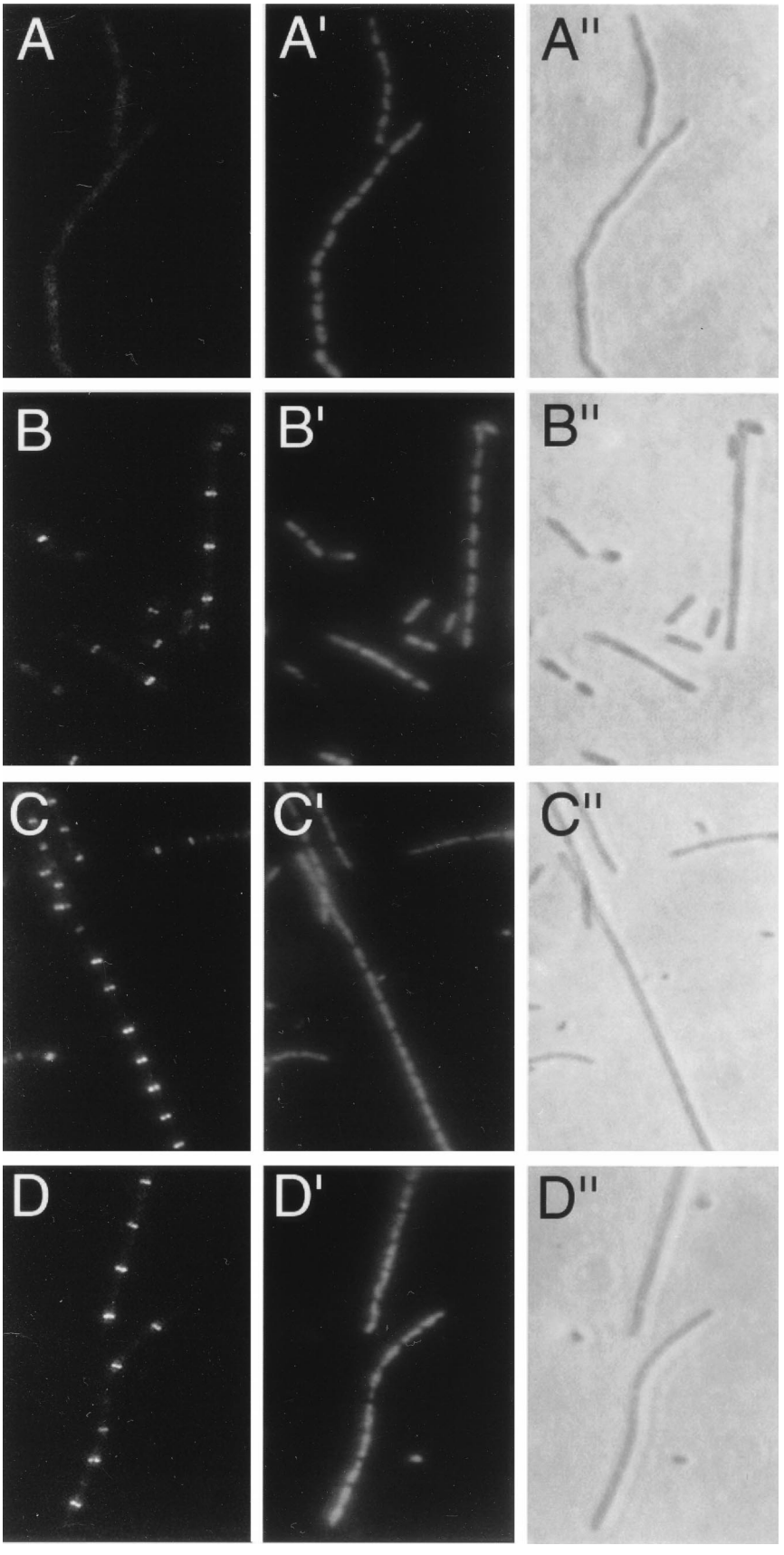

FIG. 4. Localization of FtsZ and its derivatives in JFL101 [*ftsZ84*(Ts)] cells. JFL101 derivatives containing various plasmids were grown at 42°C for 30 min, induced with 10 μM IPTG for 60 min, and then fixed for staining. Simultaneously, FtsZ was stained by anti-FtsZ and visualized by IFM (A to D), nucleoids were stained with DAPI and visualized by fluorescence microscopy (A′ to D′), and cell morphologies were visualized by phase-contrast microscopy (A″ to D″). (A to A″) JFL101 containing pWM176; (B to B″) JFL101 containing pMK4 (wild-type *ftsZ*); (C to C″) JFL101 containing pWM1202 (*ZL372A*); (D to D″) JFL101 containing pWM932 (*ZΔC1.3*).

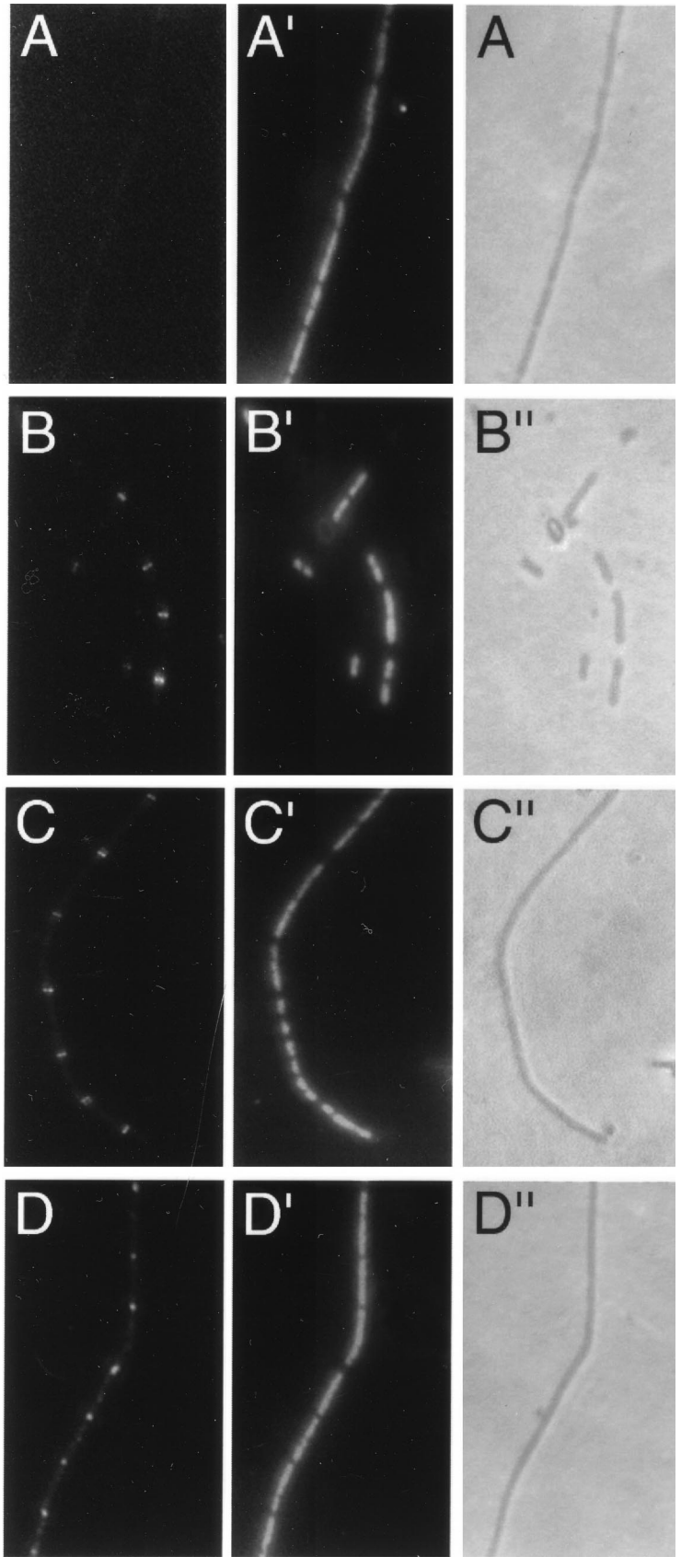

FIG. 5. Localization of FtsZ and its derivatives in WM1099 (*ftsZ* depletion strain) cells. WM1099 derivatives were grown at 42°C for 5 h before induction with 5 μM IPTG for 40 min and fixation. Simultaneously, FtsZ was stained by anti-FtsZ and visualized by IFM (A to D), nucleoids were stained with DAPI and visualized by fluorescence microscopy (A′ to D′), and cell morphologies were visualized by phase-contrast microscopy (A″ to D″). (A to A″) WM1099 containing pWM176; (B to B″) WM1099 with pMK4 (wild-type *ftsZ*); (C to C″) WM1099 with pWM1202 (*ZL372A*); (D to D″) WM1099 with pWM932 (*ZΔC1.3*).

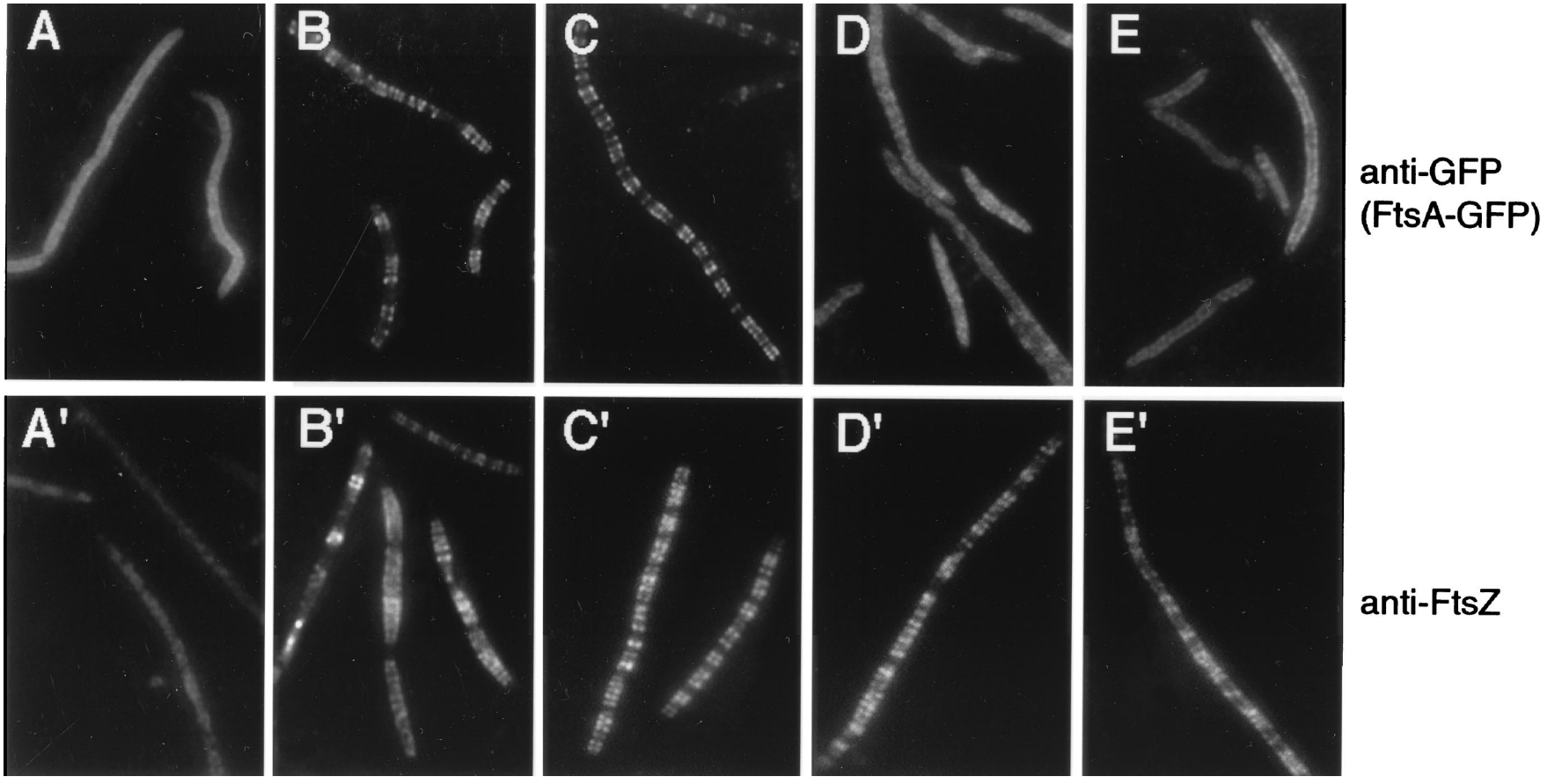

FIG. 6. Association of FtsA-GFP with FtsZ spirals in JFL101 [*ftsZ84*(Ts)]. JFL101 cells containing plasmids synthesizing FtsA-GFP and an FtsZ derivative were grown at 42°C for 30 min and then induced with 200 μM IPTG for 60 min. Parallel samples were fixed and stained with anti-GFP antibodies for FtsA-GFP and stained with anti-FtsZ antibodies for FtsZ, followed by IFM. (A to E) FtsA-GFP; (A′ to E′) FtsZ. (A and A′) WM1234 (JFL101 containing pWM633 [*ftsA*-GFP] and pWM176); (B and B′) WM1235 (pMK4 [wild-type *ftsZ*]); (C and C′) WM1242 (pWM738 [*ZD373A*]); (D and D′) WM1244 (pWM739 [*ZP375A*]); (E and E′) WM1236 (pWM737 [*ZΔC1*]).

TABLE 4. Yeast two-hybrid interaction of FtsA and FtsZ derivatives

LexA BD fusion	GAL4AD fusion	Filter assay activity[a]
FtsZ		++
	FtsZ	−
FtsA	VirE2	−
FtsA	FtsZ	++
FtsA	ZL372A	−
FtsA	ZD373A	+
FtsA	ZI374A	−
FtsA	ZP375A	−
FtsA	ZF377A	−
FtsA	ZΔC1	−
FtsA	ZΔC1.1	−
FtsA	ZΔC1.2	−
FtsA	ZΔC1.3	−
FtsA	ZΔC2	−

[a] Results of the yeast two-hybrid system are based on the color development on the filter. ++, color development within 2 h, showing strong blue; +, color development within 4 h, showing pale blue; −, no color development in 12 h.

fluorescent spirals. This was expected, because the same mutants were all able to form fluorescent rings in *ftsZ84* cells. However, anti-GFP staining revealed fluorescent FtsA-GFP spirals when FtsA-GFP was cosynthesized with ZD373A and ZL378A (Fig. 6C, showing ZD373A, and data not shown) but diffuse fluorescence with weak background patterns when cosynthesized with ZL372A and ZP375A (Fig. 6D, showing ZP375A, and data not shown). These results suggest that L372A and P375A, the two stable point mutants within the conserved core that cannot complement an *ftsZ* mutant, are also defective in efficiently interacting with FtsA-GFP.

To determine if the FtsZ-FtsA interactions measured above in cells in which FtsZ84 was thermoinactivated were similar in a strain with FtsZ depleted, we performed the interaction assays in the *ftsZ* depletion strain WM1099. FtsZ was depleted under the conditions mentioned above, followed by co-overproduction of FtsA-GFP and one of the various FtsZ derivatives. FtsA-GFP was poorly expressed in this strain with the *lac* promoter, so we used the arabinose-inducible *araBAD* promoter on plasmid pBAD30 instead. Cells harboring both this plasmid and one of the plasmids containing an *ftsZ* derivative were grown at 42°C for 5 h to deplete endogenous FtsZ and then induced with 0.2% arabinose and 10 μM IPTG for 1 h. This resulted in significantly higher production of FtsA-GFP compared to that of the FtsZ derivatives, because the *araBAD* promoter is strong and because it, unlike *lac*, is either fully repressed or fully induced in individual cells (32). As in the *ftsZ84* strain, the FtsZ C-terminal-deletion derivatives failed to interact strongly with FtsA-GFP, with anti-GFP immunostaining revealing mostly diffuse fluorescence with a weak background pattern. As expected, clear fluorescent FtsA-GFP spirals appeared in cells cosynthesizing ZD373A or ZL378A. In addition, we also occasionally observed FtsA-GFP spirals in a small fraction of cells cosynthesizing ZL372A or ZP375A (data not shown). The FtsZ/FtsA-GFP ratio in these experiments with WM099 cells was estimated by immunoblotting to be about 2 to 5, whereas JFL101 cells had a ratio of approximately 60 to 70, which is close to the estimated ratio of FtsZ to FtsA in wild-type cells (data not shown). It is possible, therefore, that the very high levels of FtsA-GFP in the WM1099 derivatives and the abnormally low FtsZ/FtsA ratio that resulted caused a significant enhancement of a normally weak protein-protein interaction.

Yeast two-hybrid analysis of FtsA interactions with mutant FtsZs. To test independently whether there was indeed a reduced interaction between FtsA-GFP and the truncated FtsZs, ZL372A, or ZP375A, as observed in the JFL101 (*ftsZ84*) strain, we used a yeast two-hybrid assay to measure FtsZ-FtsA interaction. We cloned native *ftsA* into the yeast vector pLEXA that carries the LexA DNA binding domain. Either wild-type *ftsZ* or its mutant alleles were fused in frame to the coding region of the GAL4 activation domain (GAL4AD) in pACT2.2. Combinations of the hybrid plasmids were then introduced into the yeast reporter strain L40, and the resulting cotransformants were tested for β-galactosidase activity. The pLEXA-*ftsZ* construct could not be used because of high background activity (Table 4). However, control experiments showed that cells containing pLEXA-*ftsA* and pACT2.2-*virE2* (VirE2 is an unrelated protein that is part of the *Agrobacterium tumefaciens* T-DNA transport system) did not have background β-galactosidase activity (Table 4). Cotransformants expressing both LexA-FtsA and GAL4AD-FtsZ displayed considerable β-galactosidase activity: the colonies were blue within 2 h of incubation on a filter containing X-Gal. On the other hand, when LexA-FtsA was combined with a GAL4AD fusion of any mutant FtsZ protein except ZD373A, the yeast colonies were white on the filters after overnight incubation, suggesting a lack of interaction with FtsA and the FtsZ mutant. A positive but somewhat weaker interaction (pale blue on the filter) was detected between FtsA and ZD373A (Table 4). Taken together, the results from the yeast two-hybrid assay were consistent with the *E. coli* in vivo interaction assay in the thermosensitive *ftsZ84* mutant. The data are summarized in Table 5.

Interaction between ZipA and FtsZ mutant derivatives. The interaction between ZipA and FtsZ was initially demonstrated by affinity blotting (14) and recently demonstrated by yeast two-hybrid analysis and cosedimentation (16, 30). We wanted to test whether an interaction could be detected between ZipA-GFP and FtsZ in our *E. coli* in vivo assay. As with the FtsA-GFP studies, a *zipA*-GFP fusion was cloned downstream of either the *lac* promoter in pBC or the *BADp* promoter in pBAD30 and was introduced along with pWM176 carrying *ftsZ* or its derivatives into either the *ftsZ84* thermosensitive strain JFL101 or the *ftsZ* depletion strain WM1099. Cells harboring both plasmids were grown under conditions of FtsZ inactiva-

TABLE 5. Summary of interactions between FtsA and FtsZ derivatives

Derivative[a]	Interaction with FtsA		Interaction with ZipA[d]
	E. coli in vivo assay[b]	Yeast two-hybrid[c]	
FtsZ	+	++	+
ZL372A	−	−	+
ZD373A	+	+	+
ZI374A*	−	−	−
ZP375A	−	−	+
ZF377A*	−	−	−
ZL378A	+	NT	+
ZΔC1	−	−	−
ZΔC1.1	−	−	−
ZΔC1.2	−	−	−
ZΔC1.3	−	−	−
ZΔC2	−	−	−

[a] * indicates that the FtsZ derivative is unstable.
[b] The FtsA-FtsZ interaction shown was tested in JFL101 (*ftsZ84*). +, strong fluorescent spirals; −, no strong fluorescent spirals.
[c] See legend to Table 4 for explanation of the data.
[d] The results of ZipA-FtsZ interaction shown here were examined in both JFL101 (*ftsZ84*) and WM1099 (*ftsZ* depletion) strains. NT, not tested.

tion or depletion, as described above for FtsZ-FtsA interactions, and ZipA-GFP and FtsZ were detected in cells by IFM with anti-GFP and anti-FtsZ antibodies, respectively.

When ZipA-GFP was cosynthesized with wild-type FtsZ in either JFL101 or WM1099, it exhibited fluorescent spiral structures similar to those observed with FtsA-GFP. Results from experiments in WM1099 are shown in Fig. 7, and ZipA-GFP spirals are apparent in Fig. 7B and C. ZipA-GFP was expressed at very high levels when produced from the *BADp* promoter in the depletion strain and, as a result, inhibited cell division as reported previously (14). Some cells remained filamentous even when wild-type FtsZ was cosynthesized from plasmid pMK4 (Fig. 7B′). The excess ZipA-GFP also caused a high background of staining with IFM, most easily seen in cells with FtsZ depleted (Fig. 7A and A′). However, the spiral structures could be easily distinguished from the diffuse fluorescence displayed by ZipA-GFP when it was cosynthesized with any of the truncated FtsZs (Fig. 7D, showing ZΔC1); these mutants, as explained above, exhibit a punctate pattern in the depletion strain (Fig. 7D′). When cosynthesized with the stable point mutant derivatives ZL372A, ZD373A, ZP375A, and ZL378A, ZipA-GFP and the FtsZ derivative made clear spiral patterns (Fig. 7C, showing ZP375A) that mimicked patterns formed by the FtsZ derivatives (Fig. 7C′). Therefore, ZL372A and ZP375A, which are defective in interacting with FtsA-GFP, appear to be capable of interacting with ZipA-GFP in this assay. Spirals of ZipA-GFP were not observed in cells expressing the unstable mutants ZI374A or ZF377A, and these proteins did not form spirals shown by anti-FtsZ staining.

Similar experiments were performed in the JFL101 background, in which the ZipA-GFP was expressed at lower levels from the *lac* promoter. The results were similar (Table 5), supporting the idea that ZipA-GFP, even at lower concentrations, is able to associate strongly with four of the FtsZ point mutant proteins but is unable to bind detectably to any of the truncated FtsZs, including the 12-amino-acid truncation. This C-terminal core domain of FtsZ thus appears to be essential for interaction with both FtsA and ZipA.

DISCUSSION

We have shown that the C-terminal conserved core domain of FtsZ is essential for function, because a plasmid expressing a 12-amino-acid deletion of this domain cannot complement a chromosomal *ftsZ* mutation. Additional evidence for the importance of this conserved region comes from alanine scan mutagenesis. Most of the single-residue alterations between L372 and L378, with the exception of ZD373A, cannot fully substitute for the native protein. Even cells synthesizing ZD373A as the only functional FtsZ exhibited moderate filamentation, indicating that despite its ability to allow an *ftsZ* mutant to form colonies at the restrictive temperature, this mutant FtsZ is not completely normal. Synthesis of wild-type FtsZ in the same plasmid system in the same strains, on the other hand, resulted in mostly normal-length cells.

The loss of the entire C-terminal core had a more severe effect on FtsZ function than any one of the single-amino-acid substitutions. For example, after depletion of FtsZ in WM1099, the stable point mutants of FtsZ (ZL372A, ZD373A, ZP375A, and ZL378A) assembled into rings at potential division sites within the filaments. However, the C-terminal-truncation mutants containing at least residues 1 to 316, such as ZΔC1, exhibited a regular punctate pattern within the filaments. This result indicates that they can localize to potential division sites and aggregate but cannot assemble into normal rings like the point mutants. The inability of these deleted derivatives to form normal rings was somewhat unexpected because ZΔC2, containing only residues 1 to 316, is still able to form large polymers in vitro when fused to GFP (37).

Despite their failure to form rings in the depletion strain, these C-terminally truncated FtsZs with at least residues 1 to 316 formed rings in the *ftsZ84*(Ts) mutant JFL101 at 42°C. This strain-specific difference in the behavior of the truncated FtsZs can be rationalized by partial function of the thermoinactivated FtsZ84. In JFL101, several thousand FtsZ84 proteins are estimated to be present per cell at 42°C, despite the fact that rings are not formed under these conditions. The ability to suppress this defect by overproducing FtsZ84 (27) or increasing ZipA levels (30) indicates that FtsZ84 is competent for assembly into functional rings but is less efficient at higher temperatures and requires a higher critical concentration than the wild-type protein. In our experiments, we speculate that exogenous synthesis of one of our mutant FtsZs in JFL101 at 42°C increases the total FtsZ concentration, stimulating the assembly of FtsZ84, which in turn allows the incorporation of the truncated FtsZs into a morphologically normal ring.

The ability of the stable point mutants and some of the truncated FtsZs to form rings on their own or in concert with otherwise thermoinactivated FtsZ84 indicates that the structures of these proteins are not significantly perturbed by the mutations. Moreover, dominant-negative effects were displayed by several of the mutant proteins even when present at less than wild-type levels. Such effects indicate that these mutant proteins retain normal structural motifs that allow them to interfere with the function of the native FtsZ. The most likely avenue for such interference is by coassembling with native FtsZ to form mixed rings. Why would such rings, which appear normal by fluorescence microscopy, be defective for septation? One hypothesis is that the heteropolymer cannot properly interact with a downstream protein such as FtsA. Although some of the point mutants that exhibit defects in associating with FtsA in our assays (ZL372A, ZI374A, and ZP375A) exhibit a clear dominant-negative phenotype, other mutants, such as several of the truncation mutants that are also defective in FtsA interactions, are not dominant negative. Therefore, this explanation for the phenotypes is unlikely to be correct. A defect in interacting with ZipA would also not explain the dominant-negative phenotypes because there is little correlation between these two characteristics. It is also intriguing that the smallest deletion (ZΔC1) has no dominant-negative phenotype but a larger deletion (ZΔC1.1; deletion of 23 amino acids) does and still-larger deletions (ZΔC1.2 and 1.3 and ZΔC2) do not. By inference, the dominant-negative phenotype of ZI374A may be caused by the posttranslational truncation of the protein observed on immunoblots. Although the truncation point for ZI374A is not yet established, we speculate that the resulting protein is similar in structure and function to the ZΔC1.1 truncation.

Interestingly, a 24-amino-acid C-terminal truncation of *C. crescentus* FtsZ exhibited a dominant-negative effect (12) similar to our 23-amino-acid truncation of *E. coli* FtsZ (ZΔC1.1), as well as some of our point mutants. As with our truncated *E. coli* FtsZs synthesized in cells with native FtsZ depleted, the truncated *C. crescentus* FtsZ localized in a punctate pattern in *C. crescentus* cells. Moreover, truncated *C. crescentus* FtsZ was also defective in interacting with *C. crescentus* FtsA in the yeast two-hybrid system. The similarity of these results suggests that the dominant-negative effects may have general significance. However, for the reasons mentioned above, it is unlikely that the defect in FtsZ-FtsA interactions is the cause of the dominant-negative phenotype.

The results described here suggest that the last 12 amino

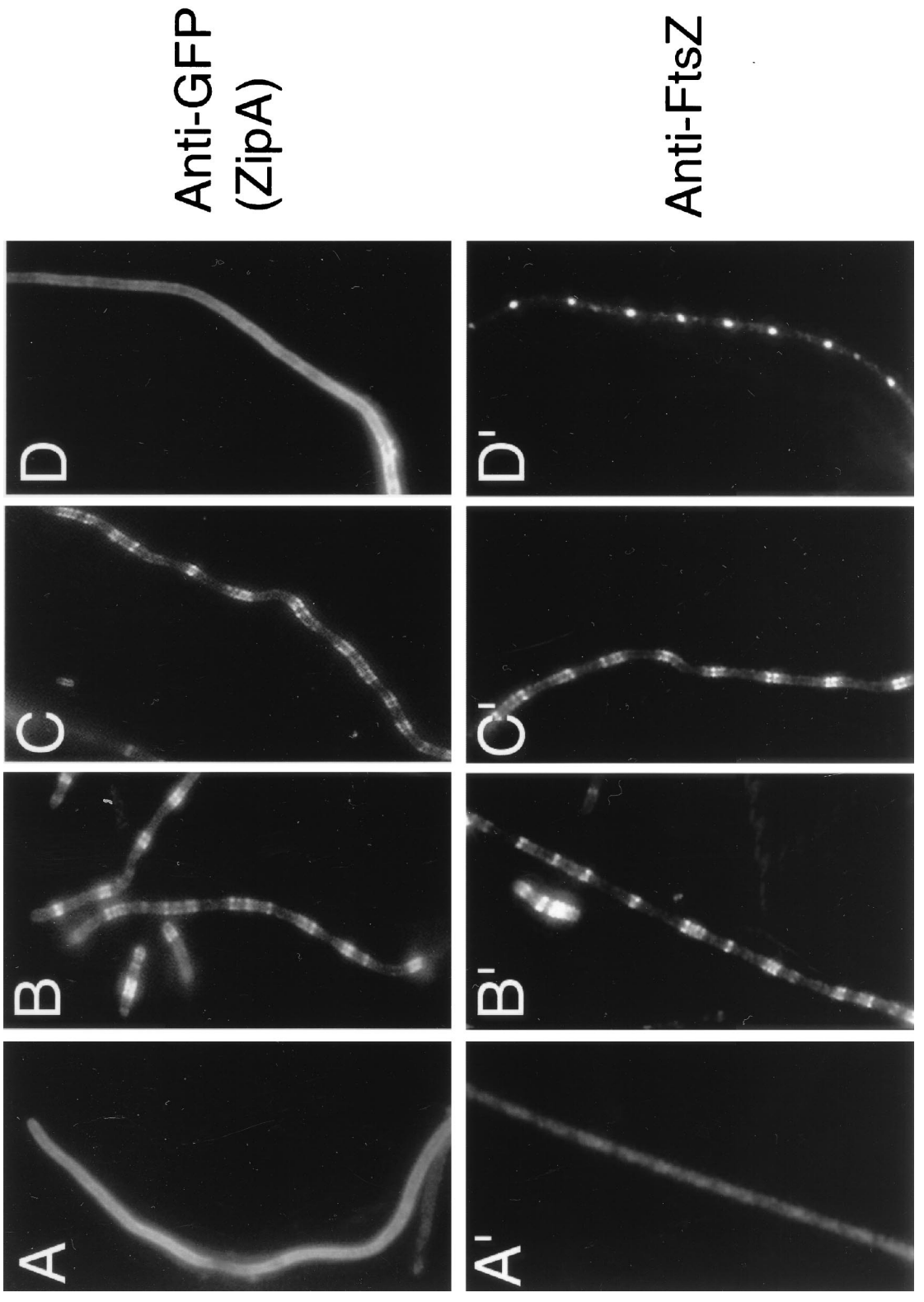

FIG. 7. Binding of ZipA-GFP to FtsZ rings and spirals in the *ftsZ* depletion strain WM1099. WM1099 containing pWM1206 (*zipA*-GFP) and various *ftsZ* derivatives were grown at 42°C for 4 h and then induced by 0.2% L-arabinose and 10 μM IPTG for 60 min. As described in the legend to Fig. 6, parallel samples were taken. One was stained with anti-GFP for ZipA-GFP and the other was stained with anti-FtsZ for FtsZ. The cells were observed by IFM for ZipA-GFP (A to D) and for FtsZ (A′ to D′). (A and A′) WM1221 (WM1099 containing pWM1206 [*zipA*-GFP] and pWM176); (B and B′) WM1222 (pWM1206 plus pMK4 [wild-type *ftsZ*]); (C and C′) WM1231 (pWM1206 plus pWM739 [*ZP3754*]); (D and D′) WM1223 (pWM1206 plus pWM737 [*ZΔC1*]).

acids of FtsZ are important for its efficient interaction with both ZipA and FtsA. This finding is consistent with the determinants of *C. crescentus* FtsZ that are needed for FtsA recruitment (12) and also with recent results implicating the C terminus of FtsZ in ZipA recruitment (16). Our studies of single-residue mutants in the C-terminal core have pinpointed two conserved residues, L372 and the invariant residue P375, that appear to have important roles in FtsA recruitment. ZipA recruitment, on the other hand, does not appear to be affected by these point mutations, suggesting that other single-residue changes may be necessary to detectably affect ZipA binding.

Our results demonstrate a correlation between noncomplementation by the FtsZ mutants and defective interaction with FtsA. However, it is not yet clear from our data or various genome sequence comparisons whether the defect in FtsA interaction is the sole reason for the noncomplementation. *Mycobacterium tuberculosis*, for example, lacks *ftsA* yet has the equivalent of L372 and P375; conversely, *Aquifex aeolicus* has *ftsA* but has only the P375 and not the L372 equivalent (Fig. 1). Our working hypothesis is that at least our C-terminal point mutants may be defective for complementation solely because they are defective for FtsA interaction. This idea seems reasonable, because these mutant proteins can (i) form rings at division sites by themselves and (ii) interact with ZipA.

The effects of ZL372A and ZP375A on the production of fluorescent spirals with FtsA-GFP were clear and reproducible with the JFL101 [*ftsZ84*(Ts)] strain. However, the results with the WM1099 depletion strain were less conclusive, as spirals were sometimes observed with all the stable point mutant FtsZs. One likely explanation for this discrepancy is that because FtsA-GFP was synthesized in the depletion strain with the strong *araBAD* promoter, FtsA-GFP levels were about 10- to 20-fold higher than those of FtsZ in the experiments with the depletion strain than with JFL101. This high level of protein may sometimes have forced an interaction between FtsA-GFP and ZL372A or ZP375A proteins that does not normally occur efficiently at lower FtsA-GFP levels. Because FtsA is normally present at 50- to 100-fold-lower levels than FtsZ, we favor the idea that the results in the JFL101 background are more physiologically relevant and that ZL372A and ZP375A are truly defective in binding to FtsA. Importantly, the yeast two-hybrid data are entirely consistent with this conclusion. Future experiments with purified proteins should allow more precise biochemical definition of the binding affinities between the various FtsZ mutants and FtsA. Such experiments should also be able to determine if the mutations in the C-terminal core disrupt an actual binding surface for FtsA and/or ZipA or instead indirectly cause structural changes in FtsZ that weaken the binding of these proteins.

Why does synthesis of high levels of FtsZ in conjunction with FtsA-GFP or ZipA-GFP result in FtsZ spirals? FtsZ spirals caused by the *ftsZ26* mutation can function normally in cell division (2), although spirals caused by overproduction of FtsZ alone (20), FtsZ-GFP, or co-overproduction of FtsZ and FtsA-GFP appear to be nonfunctional (19). The conditions controlling the assembly of spirals and their different morphologies and pitches in the cell are not known. We favor the idea that spirals represent a hyperstable form of FtsZ polymers and that ZipA and FtsA, at least when present at certain levels, are able to promote stabilization of FtsZ polymers. Biochemical and genetic evidence for such a stabilization function for ZipA has recently been reported (30). A better understanding of this phenomenon should prove useful in the design of drugs that, like taxol with microtubules, can inactivate the bacterial division system by hyperstabilizing FtsZ polymers.

ACKNOWLEDGMENTS

We thank W. Cook and L. Rothfield for the FtsZ depletion strain; X.-R. Zhou, P. Christie, J. Jones, and S. Elledge for the yeast two-hybrid vectors and advice concerning the yeast two-hybrid assay; T. Vida for help with yeast culture and transformation; and X.-C. Yu and Q. Sun for the anti-FtsZ antibody and help with the immunofluorescence assays.

This work was supported by National Science Foundation grant MCB-9513521 and National Institutes of Health Grant 1R55-GM/OD54380-01.

REFERENCES

1. **Addinall, S. G., C. Cao, and J. Lutkenhaus.** 1997. Temperature shift experiments with an *ftsZ84*(Ts) strain reveal rapid dynamics of FtsZ localization and indicate that the Z ring is required throughout septation and cannot reoccupy division sites once constriction has initiated. J. Bacteriol. **179:** 4277–4284.
2. **Addinall, S. G., and J. Lutkenhaus.** 1996. FtsZ-spirals and -arcs determine the shape of the invaginating septa in some mutants of *Escherichia coli*. Mol. Microbiol. **22:**231–237.
3. **Addinall, S. G., and J. Lutkenhaus.** 1996. FtsA is localized to the septum in an FtsZ-dependent manner. J. Bacteriol. **178:**7167–7172.
4. **Bai, C., and S. J. Elledge.** 1997. Gene identification using the yeast two-hybrid system. Methods Enzymol. **283:**141–156.
5. **Bartel, P. L., and S. Fields.** 1995. Analyzing protein-protein interactions using two-hybrid system. Methods Enzymol. **254:**241–263.
6. **Bi, E., and J. Lutkenhaus.** 1991. FtsZ ring structure associated with division in *Escherichia coli*. Nature (London) **354:**161–164.
7. **Bramhill, D., and C. M. Thompson.** 1994. GTP-dependent polymerization of *Escherichia coli* FtsZ protein to form tubules. Proc. Natl. Acad. Sci. USA **91:** 5813–5817.
8. **Chen, B., and A. E. Przybyla.** 1994. An efficient site-directed mutagenesis method based on PCR. BioTechniques **17:**657–659.
9. **Cormack, B. P., R. H. Valdivia, and S. Falkow.** 1996. FACS-optimized mutants of the green fluorescent protein (GFP). Gene **173:**33–38.
10. **Dai, K., and J. Lutkenhaus.** 1991. *ftsZ* is an essential cell division gene in *Escherichia coli*. J. Bacteriol. **173:**3500–3506.
11. **de Boer, P., R. Crossley, and L. Rothfield.** 1992. The essential bacterial cell-division protein FtsZ is a GTPase. Nature (London) **359:**254–256.
12. **Din, N., E. M. Quardokus, M. J. Sackett, and Y. V. Brun.** 1998. Dominant C-terminal deletions of FtsZ that affect its ability to localize in *Caulobacter* and its interaction with FtsA. Mol. Microbiol. **27:**1051–1063.
13. **Erickson, H. P., D. W. Taylor, K. A. Taylor, and D. Bramhill.** 1996. Bacterial cell division protein FtsZ assembles into protofilament sheets and minirings, structural homologs of tubulin polymers. Proc. Natl. Acad. Sci. USA **93:** 519–523.
14. **Hale, C. A., and P. de Boer.** 1997. Direct binding of FtsZ to ZipA, an essential component of the septal ring structure that mediates cell division in *E. coli*. Cell **88:**175–185.
15. **Hale, C. A., and P. A. de Boer.** 1999. Recruitment of ZipA to the septal ring of *Escherichia coli* is dependent on FtsZ and independent of FtsA. J. Bacteriol. **181:**167–176.
16. **Liu, Z., A. Mukherjee, and J. Lutkenhaus.** 1999. Recruitment of ZipA to the division site by interaction with FtsZ. Mol. Microbiol. **31:**1853–1861.
17. **Löwe, J., and L. A. Amos.** 1998. Crystal structure of the bacterial cell-division protein FtsZ. Nature (London) **391:**203–206.
18. **Lutkenhaus, J., H. Wolf-Watz, and W. D. Donachie.** 1980. Organization of the genes in the *ftsA-envA* region of the *Escherichia coli* genetic map and identification of a new *fts* locus (*ftsZ*). J. Bacteriol. **142:**615–620.
19. **Ma, X., D. W. Ehrhardt, and W. Margolin.** 1996. Colocalization of cell division proteins FtsZ and FtsA to cytoskeletal structures in living *Escherichia coli* cells by using green fluorescent protein. Proc. Natl. Acad. Sci. USA **93:**12998–13003.
20. **Ma, X., and W. Margolin.** Unpublished data.
21. **Ma, X., Q. Sun, R. Wang, G. Singh, E. L. Jonietz, and W. Margolin.** 1997. Interactions between heterologous FtsA and FtsZ proteins at the FtsZ ring. J. Bacteriol. **179:**6788–6797.
22. **Margolin, W.** 1998. A green light for the bacterial cytoskeleton. Trends Microbiol. **6:**233–238.
23. **Margolin, W., J. C. Corbo, and S. R. Long.** 1991. Cloning and characterization of a *Rhizobium meliloti* homolog of the *Escherichia coli* cell division gene *ftsZ*. J. Bacteriol. **173:**5822–5830.
24. **Margolin, W., and S. R. Long.** 1994. *Rhizobium meliloti* contains a novel second copy of the cell division gene *ftsZ*. J. Bacteriol. **176:**2033–2043.
25. **Mukherjee, A., K. Dai, and J. Lutkenhaus.** 1993. *Escherichia coli* cell division protein FtsZ is a guanine nucleotide binding protein. Proc. Natl. Acad. Sci. USA **90:**1053–1057.
26. **Mukherjee, A., and J. Lutkenhaus.** 1998. Dynamic assembly of FtsZ regulated by GTP hydrolysis. EMBO J. **17:**462–469.
27. **Phoenix, P., and G. R. Drapeau.** 1988. Cell division control in *Escherichia coli*

K12: some properties of the *ftsZ84* mutation and suppression of this mutation by the product of a newly identified gene. J. Bacteriol. **170:**4338–4342.
28. **Pogliano, J., K. Pogliano, D. S. Weiss, R. Losick, and J. Beckwith.** 1997. Inactivation of FtsI inhibits constriction of the FtsZ cytokinetic ring and delays the assembly of FtsZ rings at potential division sites. Proc. Natl. Acad. Sci. USA **94:**559–564.
29. **Quardokus, E., N. Din, and Y. V. Brun.** 1996. Cell cycle regulation and cell type-specific localization of the FtsZ division initiation protein in *Caulobacter*. Proc. Natl. Acad. Sci. USA **93:**6314–6319.
30. **Raychaudhuri, D.** 1999. ZipA is a MAP-Tau homolog and is essential for structural integrity of the cytokinetic FtsZ ring during bacterial cell division. EMBO J. **18:**2372–2383.
31. **Raychaudhuri, D., and J. T. Park.** 1992. *Escherichia coli* cell-division gene *ftsZ* encodes a novel GTP-binding protein. Nature (London) **359:**251–254.
32. **Siegele, D. A., and J. C. Hu.** 1997. Gene expression from plasmids containing the *araBAD* promoter at subsaturating inducer concentrations represents mixed populations. Proc. Natl. Acad. Sci. USA **94:**8168–8172.
33. **Sun, Q., and W. Margolin.** 1998. FtsZ dynamics during the cell division cycle of live *Escherichia coli*. J. Bacteriol. **180:**2050–2056.
34. **Wang, X., J. Huang, A. Mukherjee, C. Cao, and J. Lutkenhaus.** 1997. Analysis of the interaction of FtsZ with itself, GTP, and FtsA. J. Bacteriol. **179:** 5551–5559.
35. **Wang, X. D., P. A. de Boer, and L. I. Rothfield.** 1991. A factor that positively regulates cell division by activating transcription of the major cluster of essential cell division genes of *Escherichia coli*. EMBO J. **10:**3363–3372.
36. **Ward, J. E., and J. Lutkenhaus.** 1985. Overproduction of FtsZ induces minicells in *E. coli*. Cell **42:**941–949.
37. **Yu, X.-C., and W. Margolin.** 1997. Ca^{2+}-mediated GTP-dependent dynamic assembly of bacterial cell division protein FtsZ into asters and polymer networks *in vitro*. EMBO J. **16:**5455–5463.
38. **Yu, X.-C., and W. Margolin.** 1998. Inhibition of assembly of bacterial cell division protein FtsZ by the hydrophobic dye bis-8-anilino-1-naphthalenesulfonate. J. Biol. Chem. **273:**10216–10222.
39. **Yu, X.-C., and W. Margolin.** 1999. FtsZ ring clusters in *min* and partition mutants: role of both the Min system and the nucleoid in regulating FtsZ ring localization. Mol. Microbiol. **32:**315–326.